

Series solution for the image charge fields in arbitrary cylindrically symmetric Penning traps

J. V. Porto*

National Institute of Standards and Technology, Gaithersburg, Maryland 20899-8421

(Received 9 January 2001; published 29 June 2001)

This paper presents a series solution to the image charge fields of a single ion in a Penning trap. The calculation of these fields and resulting frequency shifts will be important for advances in a variety of high precision Penning trap studies, particularly for work with highly charged ions. The simple technique is applicable to cylindrically symmetric traps of otherwise arbitrary geometry and provides an efficient alternative to finite grid relaxation techniques. The present calculation is in agreement with previous measurements in a hyperbolic trap, and systematic frequency shifts for recent atomic mass measurements using multiply charged ions are given.

DOI: 10.1103/PhysRevA.64.023403

PACS number(s): 32.80.Pj, 41.20.-q, 06.30.Dr, 07.75.+h

The most accurate atomic mass measurements are made by measuring the cyclotron frequencies of individual ions in a Penning trap [1–3]. The accuracy of better than one part in 10^{10} with which atomic masses can be compared requires a detailed understanding of the trap electric and magnetic fields and their stability. As pointed out more than ten years ago [4], a possible systematic error in these measurements arises from the small image fields that are induced by the trapped ions themselves. Such image charge frequency shifts have been measured in a small trap with multiple ions [4], but they are quite small and scale as the inverse cube of the trap size. In addition, the image induced frequency shifts are independent of the ion mass to first order, depending only on the charge of the ion. When calculating the ratio of cyclotron frequencies of two equally charged ions, the *relative* frequency shift therefore depends linearly on the mass difference. This relative frequency shift for mass doublets ($\Delta m/m \approx 10^{-3}$) nearly cancels, and consequently has been safely ignored in larger single-ion mass spectrometer traps [1].

Recent measurements of alkali-metal masses at MIT [5] were made by comparing multiply charged ions to singly charged ions, for example Cs^{3+} to CO_2^+ . Estimates of the image charge frequency shifts based on a spherical model of the trap [4] indicate that for this trap the shifts are ≈ 100 μHz per charge, which is at most 30% of the total combined uncertainty of the recent measurements. Assessment of this systematic error to 10% is currently sufficient, but as the precision of future measurements increases and ions of higher charge state are used [7–9], it will be important to know the size of the image charge shifts more accurately.

Traditionally, the calculation of electrostatic trap properties in other than spherical or cylindrical traps has been handled with numerical finite grid techniques [10]. I present here a semianalytical solution for ion induced image fields that is similar to the analytical solutions available for spherical or cylindrical traps. The technique provides a series expansion for the potential near the center of the trap, which is the region of interest for trapped particle studies. It has the

advantage that it is straightforward to implement and is not computationally intensive. The technique can be applied to arbitrary cylindrically symmetric traps and a modified form of the calculation could be useful for the study and design of new traps. I start by providing a short review of the frequency shifts resulting from image fields in Penning traps, and then present the calculation of the image fields themselves.

Image charge shifts

The fields in a Penning trap and the resulting ion motions have been described in detail elsewhere [11], and I give here only a brief description necessary to provide the background for the present calculations. An ideal trap consists of a magnetic field $B_z \hat{z}$ and a cylindrically symmetric electrostatic potential

$$\Phi(\mathbf{r}) = \frac{V_0}{2} \left(\frac{z^2}{d^2} - \frac{\rho^2}{2d^2} \right) + \Phi_0, \quad (1)$$

where Φ_0 is an arbitrary constant. In a hyperbolic trap this potential (with $\Phi_0 = V_0 \rho_0^2 / 4d^2$) is created to lowest order when voltages V_0 , $V_0/2$, and 0 are applied to the endcap, guard ring, and ring electrodes of the trap, respectively. (See Fig. 1.) The guard ring electrodes are used to adjust higher-order terms in the potential. In a hyperbolic trap, the trap size d is defined by $2d^2 = z_0^2 + (\rho_0^2/2)$, where z_0 and ρ_0 are the minimum distance from the endcap and ring electrode to the center of the trap. Motion of an ion of mass m and charge q near the center of the trap separates into an axial mode and two radial modes. The frequencies of the three modes are given by

$$\omega_{z0}^2 = \frac{qV_0}{md^2},$$

$$2\omega'_{c0} = \omega_c + \sqrt{\omega_c^2 - 2\omega_{z0}^2},$$

$$2\omega_{m0} = \omega_c - \sqrt{\omega_c^2 - 2\omega_{z0}^2}, \quad (2)$$

*Electronic address: trey@nist.gov

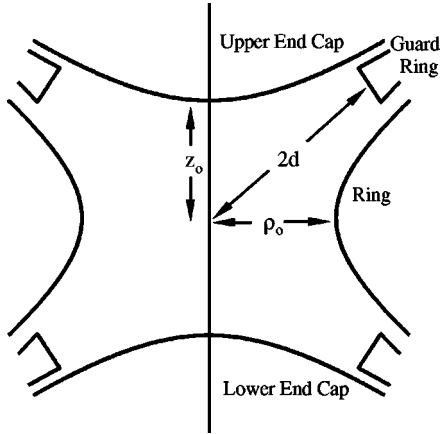


FIG. 1. Cross section of the MIT trap geometry used in these calculations. The hyperbolic electrode surfaces are determined by the equations $z^2 = z_0^2 + (\rho^2/2)$ and $z^2 = (\rho^2 - \rho_0^2)/2$. The characteristic trap size was measured to be $d = 0.55011(3)$ cm [6]. The guard ring is placed a distance $r_g = 2d$ from the center of the trap.

where $\omega_c = qB/mc$ is the free space cyclotron frequency. The three frequencies are related to ω_c by the well-known quadrature relation [11]

$$\omega_c^2 = \omega_{c0}'^2 + \omega_{z0}^2 + \omega_{m0}^2. \quad (3)$$

Using sensitive techniques [12,13], the three frequencies of a single trapped ion can be accurately measured. The free space cyclotron frequency determined from the quadrature relation (3) is the basis for high accuracy mass comparisons.

An ion in the trap induces an image charge on the inside surface of the trap, which in turn produces an electric field \mathbf{E}^{im} at the position of the ion. The induced field can perturb the ion motion and shift the trap frequencies. In general, this field will depend on the position \mathbf{r}' of the ion within the trap. During a measurement, the ion orbits are much smaller than the trap size d , and typically $|\mathbf{r}'| \leq 0.05 d$. In calculating the image shifts, it is reasonable to take only terms of lowest order in the ion position. In a cylindrically symmetric trap with vertical symmetry through the midplane, the zero-order terms vanish. The first nonzero terms in \mathbf{E}^{im} are

$$\mathbf{E}^{im}(\rho', z') \approx E_\rho^{im} \frac{\rho'}{d} \hat{\rho} + E_z^{im} \frac{z'}{d} \hat{z}, \quad (4)$$

where ρ' and z' are the radial and axial positions of the ion. The cylindrical symmetry of the trap implies that \mathbf{E}^{im} has components only in the vertical (z) and radial (ρ) directions. The next nonzero terms are therefore third order in z' and ρ' (e.g., ρ'^3 , z'^3 , $\rho'^2 z'$, or $z'^2 \rho'$) and given typical orbit sizes these terms are likely to be only about 0.25% of the first-order term.

Taking only the linear terms, the shifted ion frequencies can be determined by adding the linear image field to the usual trap fields. The derivation is almost identical to that given by Van Dyck *et al.* [4], except that the nonspherical nature of the trap is accounted for by considering E_z^{im}

$\neq E_\rho^{im}$. The result is that the measured trap frequencies are shifted from their image-free values, and are given by

$$\begin{aligned} \omega_z^2 &= \omega_{z0}^2 - \Delta_z, \\ \omega_m &= \omega_{m0} + \frac{\Delta_\rho}{\omega_c'}, \\ \omega_c' &= \omega_{c0}' - \frac{\Delta_\rho}{\omega_c'}, \end{aligned} \quad (5)$$

where

$$\Delta_{\rho,z} = \frac{qE_{\rho,z}^{im}}{md} \quad (6)$$

and ω_{z0} , ω_{m0} , and ω_{c0}' are the unperturbed axial, magnetron, and cyclotron frequencies. The quadrature relation [Eq. (3)] is also modified to give

$$\omega_c'^2 - (2\Delta_\rho + \Delta_z) = \omega_{c0}'^2 + \omega_z^2 + \omega_m^2. \quad (7)$$

Equation (7) reduces to the same expressions given by Van Dyck *et al.* [4] for a spherical trap when Δ_ρ and Δ_z are equal. [In deriving these equations, the extremely small frequency shifts $(\omega_z/\omega_c')^2(\Delta_{\rho,z}/\omega_c')$ have been ignored.] The free space cyclotron frequency, inferred from the original quadrature relation [11], is shifted down from the true frequency by

$$\delta = \frac{2\Delta_\rho + \Delta_z}{\omega_c + \sqrt{\omega_c^2 - (2\Delta_\rho + \Delta_z)}} \approx \frac{2\Delta_\rho + \Delta_z}{2\omega_c} = \frac{\left(E_\rho^{im} + \frac{1}{2}E_z^{im}\right)}{Bd/c}. \quad (8)$$

The magnetic field and trap size d can be determined from measurements of the ion frequencies. The calculation of $E_{\rho,z}^{im}$ is presented below.

Image-field calculations

The goal is to calculate the image field induced by an ion for a given position of the ion in the trap. The linearity of Maxwell's equations implies that the image field can be calculated assuming all trap electrodes are grounded. (The total field can be obtained by merely adding the image field to the static trapping fields.) In addition, we may safely ignore retardation effects, since for ions the trap size $d \approx 5$ mm is much smaller than the wavelengths associated with any of the dynamical modes of the trapped ion ($\lambda = c/f \geq 5$ m). The orientation of the coordinates is chosen so that the ion lies in the x - z plane, which in polar and spherical coordinates corresponds to the azimuthal angle $\phi' = 0$.

The electrostatic calculation is equivalent to finding the Green's function for Poisson's equation, which satisfies the Dirichlet boundary condition $qG(\mathbf{r}, \mathbf{r}') = V(\mathbf{\Omega})$ when either \mathbf{r} or \mathbf{r}' is on the surface of the electrodes. In this paper the vectors \mathbf{r} and \mathbf{r}' represent the field and ion positions, respectively, and $\mathbf{\Omega}$ represents any point on the electrode surfaces.

For the specific calculation presented here the appropriate boundary condition is $V(\mathbf{\Omega})=0$, but I will outline the calculation for arbitrary $V(\mathbf{\Omega})$ in order to demonstrate the general applicability of the solution. The Green's function can be written as the sum of the source term and an image term $F(\mathbf{r}, \mathbf{r}')$,

$$G(\mathbf{r}, \mathbf{r}') = \frac{1}{|\mathbf{r} - \mathbf{r}'|} + F(\mathbf{r}, \mathbf{r}'). \quad (9)$$

The function $F(\mathbf{r}, \mathbf{r}')$ is proportional to the image potential that we seek to calculate. It satisfies Laplace's equation and is chosen such that the boundary condition on G is satisfied. Given $F(\mathbf{r}, \mathbf{r}')$, the image field at the ion position is given by

$$\mathbf{E}^{im}(\mathbf{r}') = q \nabla_{\mathbf{r}} F(\mathbf{r}, \mathbf{r}')|_{\mathbf{r}=\mathbf{r}'}, \quad (10)$$

where the gradient is taken with respect to the field coordinates before evaluating at the position of the ion.

The general approach taken here in calculating $F(\mathbf{r}, \mathbf{r}')$ is to expand the source and image functions of Eq. (9) in a Laplace series, keeping terms of order N . The boundary condition $qG(\mathbf{\Omega}, \mathbf{r}') = V(\mathbf{\Omega})$ is then imposed approximately on the series solution by minimizing the integral of $|qG(\mathbf{\Omega}, \mathbf{r}') - V(\mathbf{\Omega})|^2$ over the surface. The set of expansion coefficients for $F(\mathbf{r}, \mathbf{r}')$ obtained from the minimization comprise the approximate solution.

Using a modified form of the addition theorem for spherical harmonics (appropriate for $r' < r$), the source term in Eq. (9) can be expanded about the origin as (setting $\phi' = 0$)

$$\begin{aligned} \frac{1}{|\mathbf{r} - \mathbf{r}'|} &= \frac{1}{d} \sum_{l=0}^{\infty} \frac{(r'/d)^l}{(r/d)^{l+1}} \left[P_l(\cos \theta) P_l(\cos \theta') \right. \\ &\quad \left. + 2 \sum_{m=1}^l \frac{(l-m)!}{(l+m)!} P_l^m(\cos \theta) P_l^m(\cos \theta') \cos m\phi \right], \end{aligned} \quad (11)$$

where the $P_l^m(x)$ are associated Legendre functions and the factor of $1/d$ is included to make the terms in the sum unitless. Since F obeys Laplace's equation, it can also be expanded in terms of Legendre functions [18],

$$F(\mathbf{r}, \mathbf{r}') = \frac{1}{d} \sum_{l=0}^{\infty} \sum_{m=0}^l C_l^m(\mathbf{r}') \left(\frac{r}{d} \right)^l P_l^m(\cos \theta) \cos m\phi. \quad (12)$$

With our choice of axes, the $\sin m\phi$ terms vanish. The arbitrary boundary condition V can be expanded in a Fourier series in the angle ϕ

$$V(\mathbf{\Omega}) = \sum_{m=0}^{\infty} V_c^m(\rho, z) \cos m\phi + V_s^m(\rho, z) \sin m\phi. \quad (13)$$

Due to the linear independence of $\sin x$ and $\cos x$, the V_c^m and V_s^m terms can be handled separately. For simplicity in the following discussion, I will consider only the $\cos m\phi$ terms, but the general approach is similar for the $\sin m\phi$ terms. The

set of dimensionless coefficients $C_l^m(\mathbf{r}')$ is to be determined from the condition $qG(\mathbf{\Omega}, \mathbf{r}') \approx V(\mathbf{\Omega})$.

The entire ϕ dependence of each term is contained in $\cos m\phi$. Since $\cos m\phi$ and $\cos m'\phi$ are linearly independent for $m \neq m'$, each sum over l at fixed m must vanish independently. Regrouping the same- m terms in Eq. (11) and (12) and summing over l gives a separate boundary condition equation for each m . Dropping the common factor $\cos m\phi$ and truncating the sum at N gives the set of equations at $\mathbf{r} = \mathbf{\Omega}$

$$\begin{aligned} \frac{q}{d} \sum_{l=0}^N \left[\frac{(r'/d)^l}{(r/d)^{l+1}} P_l(\cos \theta') + C_l^0(\mathbf{r}') \left(\frac{r}{d} \right)^l \right] P_l(\cos \theta) \\ = V^0(\mathbf{r}), \quad m=0, \end{aligned} \quad (14)$$

$$\begin{aligned} \frac{q}{d} \sum_{l=m}^N \left[2 \frac{(l-m)!}{(l+m)!} \frac{(r'/d)^l}{(r/d)^{l+1}} P_l^m(\cos \theta') + C_l^m(\mathbf{r}') \left(\frac{r}{d} \right)^l \right] \\ \times P_l^m(\cos \theta) = V^m(\mathbf{r}), \quad m \neq 0. \end{aligned} \quad (15)$$

For a given N , approximate solutions ${}^N C_l^m(\mathbf{r}')$ can be determined by minimizing the integral of the square of the sums (14) and (15), which for $m=0$ looks like

$$\begin{aligned} \int_S \left| \sum_{l=0}^N \left[\frac{(r'/d)^l}{(r/d)^{l+1}} P_l(\cos \theta') + C_l^0(\mathbf{r}') \left(\frac{r}{d} \right)^l \right] P_l(\cos \theta) \right. \\ \left. - \frac{d}{q} V^0(\mathbf{r}) \right|^2 d\Omega. \end{aligned} \quad (16)$$

The integral is over the unprimed variables constrained to the electrode surfaces. With m fixed, the integral is essentially one-dimensional. The minimum of the integrals is determined in the standard way by setting the derivative with respect to a particular $C_k^m(\mathbf{r}')$ equal to zero. Interchanging the order of the summation and integral results in the following set of $N-m$ linear equations for each m (I have temporarily dropped the indices N and m for convenience)

$$B_{kl} C_l(\mathbf{r}') + D_{kl} A_l(\mathbf{r}') - V_k = 0, \quad (17)$$

where summation over repeated indices extends from $l=m$ to N , and

$$A_l(\mathbf{r}') = \left(\frac{r'}{d} \right)^l P_l^m(\cos \theta'), \quad (18)$$

$$B_{kl} = \int_S \left(\frac{r}{d} \right)^{l+k} P_l^m(\cos \theta) P_k^m(\cos \theta) d\Omega, \quad (19)$$

$$V_k = \frac{d}{q} \int_S V^m(\mathbf{r}) \left(\frac{r}{d} \right)^k P_k^m(\cos \theta) d\Omega, \quad (20)$$

and

$$m=0: \quad D_{kl} = \int_S \left(\frac{r}{d} \right)^{k-l-1} P_l(\cos \theta) P_k(\cos \theta) d\Omega,$$

$$m \neq 0: \quad D_{kl} = 2 \frac{(l-m)!}{(l+m)!} \int_S \left(\frac{r}{d} \right)^{k-l-1} P_l^m(\cos \theta) \times P_k^m(\cos \theta) d\Omega. \quad (21)$$

Inverting B_{kl} in Eq. (17) gives the formal solution

$$C_l(\mathbf{r}') = C_{lk} A_k(\mathbf{r}') + B_{lk}^{-1} V_k, \quad (22)$$

with $C_{lk} = -B_{ij}^{-1} D_{jk}$. Given the symmetry of the Legendre functions, the integrals for B_{kl} and D_{kl} vanish unless l and k are either both even or both odd. Since the even and odd terms do not mix, B and D can be split and the parts with different symmetry solved separately. An approximate solution of mixed symmetry but fixed m therefore consists of calculating $N^2 + N$ integrals ($N^2/4$ for each symmetry of B and D and N for V_k) and inverting two symmetric $N/2 \times N/2$ matrices. In the absence of source terms, the coefficients C_l are independent of \mathbf{r}' and only $N^2/2 + N$ integrals must be calculated.

The solution given by Eqs. (12) and (22) depends implicitly on the number of terms N included in the sum. It is only meaningful if it converges fast enough with increasing N . Since we are interested in the potential near the center of the trap, we only need to calculate the lowest-order terms of C_{kl} . Certainly, since $|\mathbf{r}'|$ is small, the first few $A_k(\mathbf{r}')$ should be sufficient, which implies that only the first few columns of D_{kl} need be calculated. One may be concerned, however, that in the integrals defining B_{kl} and D_{kl} the field position $|\mathbf{r}| = |\mathbf{\Omega}|$ is not small, indicating that an accurate solution may require a large number of terms. In addition, the inversion of B_{kl} requires it to be sufficiently well conditioned so that inversion does not introduce significant errors. For a spherical trap, the size of $|\mathbf{\Omega}|$ and the inversion of B_{kl} are not an issue because the different P_l^m are orthogonal and B and D are therefore diagonal. In a nonspherical trap, however, this is not the case.

The condition number of a matrix, K , provides a measure of how sensitive matrix inversion is to errors [14]. An approximate form of the condition number is given by $K(A) = n [A_{ij}]_{\max} [A_{ij}^{-1}]_{\max}$, where n is the order of the matrix and $[A_{ij}]_{\max}$ is the maximum element of A . For the hyperbolic trap geometries used here, direct calculation shows that the condition number $K(^N B)$ grows exponentially with N , indicating that $^N B$ is increasingly ill-conditioned. As a result, the requirements on the numerical precision of the integrals in Eqs. (19) become very stringent as N increases. If the series does not converge sufficiently quickly at a given precision, the problem may become numerically unstable before a solution can be obtained. Fortunately, this can easily be checked and for all the calculations presented here the procedure was found to be robust at standard double precision up to $N=44$ (corresponding to 22 terms). The solution was typically within 0.1% of the limiting value by $N=16$.

Before proceeding to the image charge shifts, I point out some useful properties of the solution given by Eq. (22). While the integrals B_{kl} and D_{kl} depend on the geometry of the trap surface, they are *independent* of the boundary con-

dition $V(\mathbf{\Omega})$ on that surface. The boundary condition is determined entirely by the N integrals V_k . This means that once all the B_{kl} have been calculated for a fixed trap geometry, calculating the trap field for an arbitrary boundary condition requires only N additional integrals, which is significantly faster than the full calculation. The relaxation technique requires a full separate calculation for each new boundary condition, even at fixed geometry. This could be particularly convenient in designing traps and understanding the contribution of each part of the trap to the potential at the trap center. For example, taking $V(\mathbf{r}) = \delta(\mathbf{r} - \mathbf{r}_o)$ (where \mathbf{r}_o is an arbitrary point on the electrode surface) gives the contribution of the point \mathbf{r}_o to the trap fields and does not require any integration. This can be used to decide how best to section a given trap into electrodes or how trapped surface charges at different positions affect the trap fields.

Another useful property of this technique is that there is some freedom in choosing the approximate boundary conditions. The boundary condition $|qG(\mathbf{\Omega}, \mathbf{r}') - V(\mathbf{\Omega})|^2 = 0$ can be multiplied by a nonzero weighting function $w(\mathbf{r})$. In the limit $N \rightarrow \infty$ the solution for $G(\mathbf{r}, \mathbf{r}')$ should be independent of $w(\mathbf{r})$. With some knowledge of the solution, the freedom to choose $w(\mathbf{r})$ can be used to emphasize different parts of the trap and improve the convergence of the solution. For example, in the image charge calculations presented here, each point on the electrode surfaces does not contribute equally to the total image field at the center. In fact, the image field contribution of a surface point scales as the inverse cube of the distance to the center of the trap, $1/r^3$ [4]. Choosing a weighting function $w(\mathbf{r}) \propto 1/r^3$ relaxes the boundary condition on distant parts of the trap in such a way that errors in the approximate solution of $G(\mathbf{r}, \mathbf{r}')$ contribute equally from all parts of the trap. It is important to note that the choice of $w(\mathbf{r})$ does not affect the value of the converged solution (assuming it converges), only the number of terms needed to reach convergence. This was confirmed by performing calculations with and without $w(\mathbf{r})$.

The lowest-order coefficients of $F(\mathbf{r}, \mathbf{r}')$ relevant for the image shift ($V_k = 0$) are given by

$$F(\mathbf{r}, \mathbf{r}') \simeq \frac{1}{d^3} \left[C_{11}^0 z z' + C_{11}^1 \rho \rho' + C_{20}^0 \left(z^2 - \frac{\rho^2}{2} \right) \right]. \quad (23)$$

Taking the gradient [Eq. (10)] and comparing with Eq. (4), the image fields are given by

$$E_z^{im} = \frac{q}{d^2} (C_{11}^0 + 2C_{20}^0), \quad E_\rho^{im} = \frac{q}{d^2} (C_{11}^1 - C_{20}^0). \quad (24)$$

The resulting frequency shift is given by

$$\delta = \frac{qc}{Bd^3} \left(C_{11}^1 + \frac{1}{2} C_{11}^0 \right), \quad (25)$$

which is independent of the ion mass and linear in the ion charge. [The C_{20}^0 term does not contribute to the total frequency shift, since it adds to the overall potential in exactly the same way that the trap electrodes do. It is equivalent to a

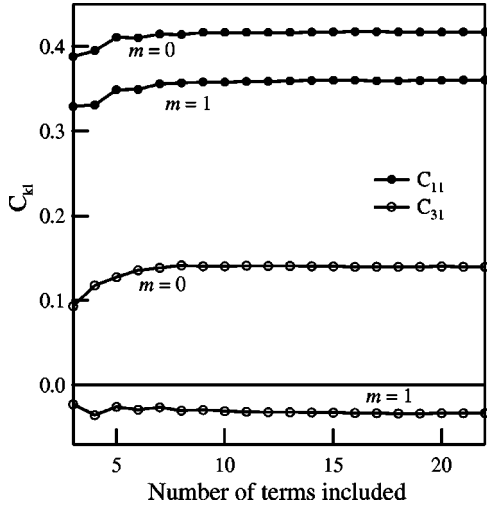


FIG. 2. The image field expansion coefficients C_{kl}^m and C_{3l}^m as a function of the number of terms included in the calculation. The calculation was performed for the hyperbolic geometry shown in Fig. 1 with all electrodes grounded.

slight shift in the trapping potential V_0 , and is therefore accounted for by the quadrature relation (3).]

The integrals (19) and (21) were performed numerically and the B_{kl} were inverted using standard routines. For most geometries at standard double precision, up to 22 terms ($N=44$) were included without instability in the inversion of B_{kl} . On the other hand, including only three terms in the calculation gives C_{11}^0 and C_{11}^1 to within 8% of the limiting value. Including only seven terms gives C_{11}^0 and C_{11}^1 to within 0.5% of the limiting value. For higher N the relative error continues to decrease, but more slowly, as shown in Fig. 2. One property of the series solution is that it can accurately approximate the potential near the trap center without having to account for the exact fields everywhere in the trap. This can be seen in Fig. 3, which compares the exact source potential $q/|\mathbf{r}-\mathbf{r}'|$ to the induced potential $-qF_N(\mathbf{r},\mathbf{r}')$ at the trap surface. In the limit $N \rightarrow \infty$, the approximate image potential $F(\mathbf{r},\mathbf{r}')$ should cancel the exact source potential everywhere on the electrode surface. Despite the relatively poor agreement at the surfaces when only seven terms are included, the lowest-order term (which governs the potential at the center of the trap) is already quite accurate. Extending the series solution to 22 terms significantly improves the agreement at the surface, but only changes the first-order terms by 0.5%.

As an additional check on the consistency of the calculation, the expansion coefficients for a source-free cylindrical trap ($D_{kl}=0$) were computed and compared to the known exact solution [15]. Unit potentials were applied to either the ring (even- z symmetry) or the upper endcap (odd- z symmetry), and the approximate solutions were determined as a function of the number of terms included. The results are plotted in Fig. 4 for the even- z symmetry. Similar convergent behavior was found, and by including 7 terms the lowest-order coefficients were within 0.2% of the exact solution. The accuracy of 5×10^{-5} obtained for $N=44$ is comparable to the typical uncertainty arising from the measured trap size d .

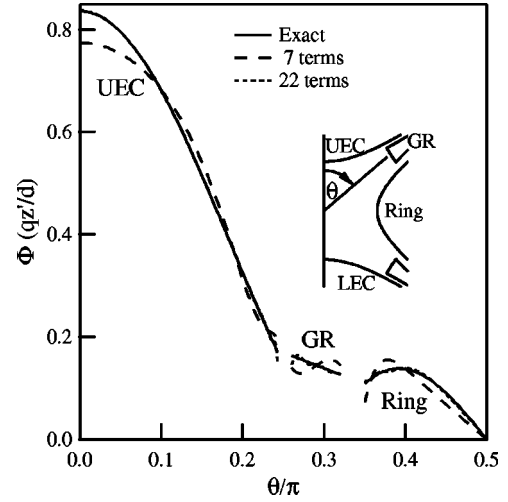


FIG. 3. The exact source potential $q/|\mathbf{r}-\mathbf{r}'|$ and the approximate image potential $-qF(\mathbf{r},\mathbf{r}')$ evaluated at the the trap surface. The calculation was performed with $m=0$, which corresponds to a source charge lying on the z -axis, $\rho'=0$. (The scaled potential $\Phi/(qz'/d)$ is independent of z' in the limit of small z' .)

In order to compare the calculation to experimental measurements, it is convenient to determine the radius of an equivalent spherical trap. The frequency shift for a spherical trap of radius a is [4]

$$\delta = \frac{3}{2} \frac{qc}{Ba^3}. \quad (26)$$

Comparing expressions (25) and (26), the radius of an equivalent spherical trap is given by

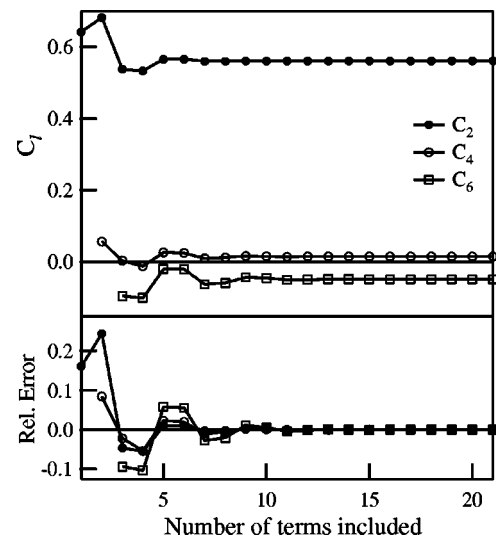


FIG. 4. The source-free expansion coefficients for a cylindrical trap with the ring electrode held at 1 Volt and the upper endcap grounded. The error is relative to the exact analytical result C_l : $(^N C_l - C_l)/C_l$. The aspect ratio was taken to be $\rho_0/z_0=1.16$.

$$a = d \left[\frac{3}{2} \frac{1}{C_{11}^1 + C_{11}^0/2} \right]^{1/3}. \quad (27)$$

Van Dyck *et al.* [4] measured the effective sphere radius for a small hyperbolic trap. The present technique was applied to the specific geometry of their trap, resulting in the coefficients $C_{11}^0 = 0.511$, $C_{11}^1 = 0.298$, and $C_{20}^0 = 0.137$. The exact details of the guard ring were not known, so an approximation of its position was made, but the guard ring does not contribute significantly to the frequency shift. The spherical approximation $\Delta_\rho = \Delta_z$ is inadequate for this trap, since $\Delta_\rho \approx 0.2\Delta_z$. The calculated effective sphere radius is $a = 1.394d = 0.995\rho_0$, which is in very good agreement with the measured value of $a = 0.99(6)\rho_0$.

The calculation was applied to the MIT trap geometry, and the resulting coefficients are given by

$$\begin{aligned} C_{11}^0 &= 0.4174(3), \\ C_{11}^1 &= 0.3603(4), \\ C_{20}^0 &= 0.0629(5). \end{aligned} \quad (28)$$

The MIT trap geometry is slightly more spherical, since C_{20}^0 is closer to zero and the difference between C_{11}^0 and C_{11}^1 is smaller, but Δ_ρ is still only about half of Δ_z . The errors are estimates based solely on the scatter in the solution obtained for $16 < N < 44$, assuming that the series is converging accurately. For the recent alkali measurements [5], [$d = 0.55011(3)$ cm, $B = 8.529 \times 10^4$ gauss] this gives a frequency shift of $\Delta f_c = \delta/2\pi = 91.84(7)$ μ Hz per charge. Errors in δ arising from uncertainties in the trap size, $\Delta\delta/\delta = 3\Delta d/d$, can be determined from the slope of the linear relationship between the applied voltage and the axial frequency, $\omega_z^2 = qV_0/md^2$, for ions of different q/m . Measuring the slope avoids problems caused by unknown offsets in the applied voltage V_0 . The accuracy is typically limited by the uncertainty in the voltage measurement to a few parts in 10^5 , which is still much smaller than the theoretical contribution to the overall uncertainty. Errors in δ arising from uncertainties in the radial position r_g of the guard ring were estimated from calculations at different r_g . As expected, the coefficients C_{kl} were found to depend exponentially on r_g [17],

but the total contribution was less than 0.2% for the MIT geometry. At $r_g = 2d$ the differential dependence $\partial C_{kl}/\partial r_g$ was about -0.003 , so that a 1% error in r_g contributes 1.4×10^{-4} to the overall error. The error in the frequency shift is dominated by uncertainties in the present calculation, but is still of sufficient accuracy to be adequate in the foreseeable future.

In closing, I point out that it may be possible to extend this technique beyond the long wavelength electrostatic limit to shorter wavelengths, which would be applicable to the cavity induced frequency shifts found in trapped electron studies. In such a solution, the Green's function for the Poisson equation would be replaced by the Green's function for the Helmholtz equation, resulting in spherical Bessel function expansions [16] instead of the usual Legendre functions. The vector nature of the time-dependent solution complicates the boundary conditions, but the problem appears to be readily tractable if the independent scalars $\mathbf{r} \cdot \mathbf{B}$ and $\mathbf{r} \cdot \mathbf{E}$ are used as solutions to the Helmholtz equation [16]. Each solution of this type could provide both the size and shape of the fields in a hyperbolic trap for a given frequency ω . There are, of course, a number of significant problems that may prevent the time-dependent series solution from being useful. Unlike the static case, where fields at the trap center are not very sensitive to some of the exact details of the trap electrodes, the dynamic solution near resonances is quite sensitive to the electrode geometry and the boundary conditions on the surface. This will probably make the issues associated with proper convergence worse for the time-dependent case. In addition, it is not clear how difficult it will be to incorporate the effects of damping (or skin depth) on the boundary conditions in the trap. As has been pointed out [17], this problem is not just theoretical in nature, since uncertainties in trap construction lead to uncertainties in the mode structure of the trap. In general, the construction of accurate hyperbolic traps is much more difficult than cylindrical traps. Nevertheless, an efficient method for short wavelength trap calculations for arbitrary cylindrically symmetric geometries would be useful, and it seems to be worth investigating.

I would like to thank D.E. Pritchard and J.D. Gillaspay for support for thinking about ion traps, and J. K. Thompson, S. Rainville, and M. P. Bradley for helpful discussions.

-
- [1] F. D'Filippo, V. Natarajan, K.R. Boyce, and D.E. Pritchard, *Phys. Rev. Lett.* **73**, 1481 (1994).
[2] D.L. Farnham, R.S. Van Dyck, and P.B. Schwinberg, *Phys. Rev. Lett.* **75**, 3598 (1995).
[3] G. Gabrielse, A. Khabbaz, D.S. Hall, C. Heimann, H. Kalinowsky, and W. Jhe, *Phys. Rev. Lett.* **82**, 3198 (1999).
[4] R.S. Van Dyck, F.L. Moore, D.L. Farnham, and P.B. Schwinberg, *Phys. Rev. A* **40**, 6308 (1989).
[5] M.P. Bradley, J.V. Porto, S. Rainville, J.K. Thompson, and D.E. Pritchard, *Phys. Rev. Lett.* **83**, 4510 (1999).
[6] J. K. Thompson (private communication).
[7] T. Beier, I. Lindgren, H. Persson, S. Salomonson, P. Sunnergren, H. Häffner, and N. Hermanspahn, *Phys. Rev. A* **62**, 032510 (2000).
[8] H. Häffner, N. Hermanspahn, P. Indelicato, H.J. Kluge, E. Lindroth, V. Natarajan, W. Quint, S. Stahl, J. Verdu, and G. Werth, *Hyperfine Interact.* **127**, 271 (2000).
[9] H. Borgenstrand *et al.*, *Phys. Scr.* **T71**, 88 (1997).
[10] G. Gabrielse, *Phys. Rev. A* **27**, 2277 (1983).
[11] L.S. Brown and G. Gabrielse, *Rev. Mod. Phys.* **58**, 233 (1986).
[12] E.A. Cornell, R.M. Weisskoff, K.R. Boyce, and D.E. Pritchard, *Phys. Rev. A* **41**, 312 (1990).
[13] F.L. Moore, L.S. Brown, D.L. Farnham, S. Jeon, P.B.

- Schwinberg, and R.S. Van Dyck, *Phys. Rev. A* **46**, 2653 (1992).
- [14] G. Arfken, *Mathematical Methods for Physicists* (Academic Orlando, 1985).
- [15] G. Gabrielse and F.C. Mackintosh, *Int. J. Mass Spectrom. Ion Processes* **57**, 1 (1984).
- [16] J.D. Jackson, *Classical Electrodynamics* (Wiley, New York, 1975).
- [17] L.S. Brown, G. Gabrielse, J. Tan, and K.C.D. Chan, *Phys. Rev. A* **37**, 4163 (1988).
- [18] Many authors include a factor of 1/2 in similar definitions of the field expansion. In order to be consistent with the expansion for $1/|\mathbf{r}-\mathbf{r}'|$, the factor 1/2 is not included here, so the coefficients C_l^m may differ by a factor of 2 from other treatments of similar problems.